ACS Photonics

Article

pubs.acs.org/journal/apchd5

Saturation and Reverse Saturation of Scattering in a Single Plasmonic Nanoparticle

Shi-Wei Chu,*[,†,‡] Hsueh-Yu Wu,[†] Yen-Ta Huang,[†] Tung-Yu Su,[†] Hsuan Lee,[†] Yasuo Yonemaru,[§] Masahito Yamanaka,[§] Ryosuke Oketani,[§] Satoshi Kawata,[§] Satoru Shoji,[§] and Katsumasa Fujita*[,§]

[†]Department of Physics and [‡]Molecular Imaging Center, National Taiwan University, Taipei 10617, Taiwan R.O.C

[§]Department of Applied Physics, Osaka University, Osaka, Japan

ABSTRACT: Nonlinear optical interaction is crucial to all-optical signal processing. In metallic nanostructures, both linear and nonlinear optical interactions can be greatly enhanced by surface plasmon resonance (SPR). In the last few decades, saturation and reverse saturation of absorption in plasmonic materials have been unraveled. It is known that scattering is one of the fundamental light−matter interactions and is particularly strong in metallic nanoparticles due to SPR. However, previous methods measure response from ensemble of nanoparticles and did not characterize scattering on a single particle basis. Here we report that backscattering from an isolated gold nanoparticle exhibits not only saturation, but also reverse saturation. Wavelength-dependent and intensity-dependent studies reveal that nonlinear scattering is dominated by SPR and shares a similar physical origin with nonlinear absorption. The reversibility and repeatability of saturable scattering (SS) and reverse saturable scattering (RSS) are validated via repetitive excitation on the same set of particles. Compared to fluorescence, our novel discovery of single-particle-based SS and RSS does not suffer from bleaching and can be used as a more robust contrast agent for optical microscopy. Under a reflection confocal microscope, interesting point-spread functions are observed, with full-width-of-half-maximum of central and side lobes reduced to $\lambda/5$ and $\lambda/13$, showing great potential for superresolution microscopy.

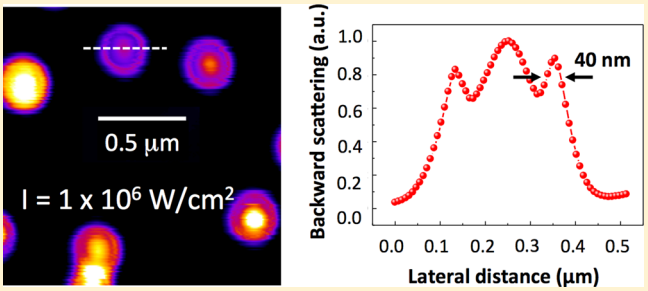

KEYWORDS: *confocal microscopy, surface plasmon resonance, metallic nanostructure, nonlinearity of scattering, point spread function, resolution*

The study of plasmonics has recently attracted extensive interest because it provides light manipulation capability on a nanometer scale for photonic integrated circuits, nano laser, biosensing, and near-field super-resolution imaging applications.[1−4] Adding nonlinearity to the field of plasmonics enables even more application possibilities. Typically, metal possess much larger third-order nonlinearity than dielectric materials. For example, the Kerr coefficient of gold is about 10^{-8} esu, which is 10^6 times more than fused silica.[5] A very nice recent review of nonlinear plasmonics can be found here.[6] One of the most studied nonlinearities in plasmonic materials is saturable absorption (SA), that is, the absorption coefficient becomes smaller when the excitation intensity increases.[7,8] Interestingly, when the excitation intensity further increases, the absorption coefficient would rise up again, showing the effect of reverse saturable absorption (RSA).[9,10] The SA and RSA properties can be applied to optical switching and optical limiting, and has found applications in all-optical signal processing.[11]

However, most of the previous SA and RSA experiments were carried out using a *z*-scan technique as ensemble measurement in bulk materials, where plasmonic particles were embedded in dielectric media. It is very difficult to identify absorption from a single plasmonic particle with conventional *z*-scan technique, unless with a sophisticated setup under an optical microscope.[12]

To determine the optical response of a single nanoparticle, we note that when light illuminates a metal film, most of the light is not absorbed, but reflected. This is very similar to the case of plasmonic nanoparticle, whose scattering is extraordinarily strong. It is known that the scattering of a single plasmonic particle can be easily detected under a microscope, with a dark-field or a reflection confocal scheme. In addition, in plasmonic nanoparticles, the absorption and scattering are linked via Mie theory.[13] Therefore, the aim of this work is to characterize the nonlinearity of scattering from an isolated plasmonic nanoparticle. We found that backscattering of a single gold nanoparticle exhibit both saturation and reverse saturation behaviors. In addition, under a confocal microscope, very interesting shape change of point-spread-function (PSF) was observed due to the nonlinearity of scattering. The width of the PSF is significantly reduced, showing great potential for high-resolution microscopy.

Under the constraint of dipolar oscillation of the free electrons in the conduction band, the absorption cross-section

Received: September 3, 2013
Published: November 12, 2013

from a plasmonic nanoparticle can be determined by classical Mie theory as[13]

$$C_{abs} = 4\pi k r^3 \mathrm{Im}\frac{\varepsilon_p - \varepsilon_m}{\varepsilon_p + 2\varepsilon_m} \quad (1)$$

where k is the wave vector, r is the radius of particle, ε_p is the dielectric constant of the particle, and ε_m is the dielectric constant of the surrounding medium. On the other hand, the scattering cross-section can be written as

$$C_{sca} = 8\pi k^4 r^6 \left|\frac{\varepsilon_p - \varepsilon_m}{\varepsilon_p + 2\varepsilon_m}\right|^2 \quad (2)$$

What conventional z-scan measured is in fact the extinction, which combines both absorption and scattering. Qualitatively, when the plasmon absorption band "bleaches" (i.e., hot electrons modify the dielectric properties of nanoparticle),[14] the refractive index of the nanoparticle changes, resulting in the saturation of absorption. Since the equation of scattering cross-section contains the same terms with the equation of absorption cross-section, it is natural to expect saturation of scattering when the absorption starts to saturate. It should be emphasized that compared to z-scan, which measures collective behavior of nanoparticles and mixed the contribution of scattering loss and absorption loss together, here we determine pure back-scattered signal on a single particle basis.

The experimental setup is a standard reflection confocal laser-scanning microscope (CLSM). To compare the wavelength dependence of scattering saturation, four continuous-wave laser sources are used, with wavelengths at 405, 532, 561, and 671 nm. Two-dimensional raster scanning was achieved with a set of galvo-mirrors. An oil-immersion 60× objective with numerical aperture (NA) equal to 1.42 is used for both excitation and collection of scattering signals. The scattering signal was detected by a photomultiplier tube (PMT) after a pinhole, and images were formed by synchronizing the PMT signal and the scanner.

Figure 1a shows the white-light backscattering spectrum of a single 80 nm gold nanoparticle in oil. A clear plasmonic peak is observed around 570 nm, which matches very well to the Mie theory prediction. We have tried several different wavelengths as excitation sources to examine the nonlinearity of scattering. The scattering of an individual particle is measured under a reflection confocal microscope. Among the wavelengths, 405 nm is outside the plasmonic band, 671 nm locates around the tail of the plasmonic band, 532 nm is close to the plasmonic resonance peak, and 561 nm is almost right on the peak. The intensity dependence of scattering versus excitation with 561 nm excitation is shown in Figure 1b, where the trend of saturation and reverse saturation is evident. The inset of Figure 1b provides the spectrum of backward signal measured right in front of the PMT. Only a narrow peak at 561 nm is observed, ensuring no luminescence component in our experiment.

To compare with experimental results of saturable absorption,[9] where transmittance (ratio of transmitted power over incident power) is measured, we used the scattering cross-section, which is proportional to the ratio of scattering over excitation intensity, to quantify the results, as shown in Figure 1c. In both Figures 1b and c, when laser intensity is less than 10^5 W/cm^2, scattering intensity is linearly dependent on excitation intensity, as shown by the blue dashed lines. When laser intensity increases over 10^5 W/cm^2, the scattering cross-section quickly decreases, indicating the saturation of scattering. In Figure 1c, an arrow shows the location of the saturation intensity, which is defined as the excitation intensity that makes scattering cross-section becomes half of the small-signal value. The saturation intensities of different wavelengths are marked in Figure 1d. It is obvious that the closer the excitation wavelength to the plasmonic resonance peak, the smaller is the required saturation intensity. It is interesting to notice that, although 405 nm laser exhibits strong attenuation for 80 nm gold nanoparticles, there is no saturation behavior at all for this wavelength, even up to the intensity of 5×10^7 W/cm^2. We believe it is because 405 nm is located outside the SPR band. The result suggests that saturable scattering (SS) is dominated by plasmon resonance of the gold nanoparticles.

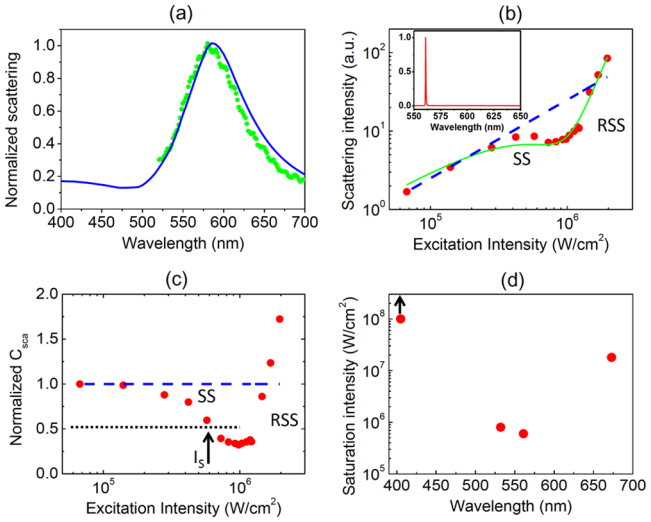

Figure 1. (a) White-light backscattering spectrum of an individual 80 nm gold nanoparticle, showing SPR peak around 550 nm. The green circles are experimentally measured data, and the blue solid line represents simulation based on Mie theory. (b) The red circles present nonlinear dependence of scattering on 561 nm excitation. When the excitation intensity is low, the scattering intensity is linearly proportional to excitation intensity. When the excitation intensity exceeds 2×10^5 W/cm^2, scattering deviates from linear trend, which is depicted by the blue dashed line. When the excitation intensity is higher than 10^6 W/cm^2, the scattering quickly increases to exceed the linear trend, showing the reverse saturation of scattering. The green line is the theoretical fitting based on nonlinear scattering equation $I_{sca} = \alpha I + \beta I^2 + \gamma I^3$. The inset shows the backward spectrum from a single nanoparticle measured in front of the PMT. Only backscattering with a narrow line width is observed. (c) The normalized scattering cross-section variation versus 561 nm excitation intensity. If scattering is linearly proportional to excitation, the scattering cross-section should be fixed at unity, as shown by the blue dashed line. Saturation is obvious when the data points deviates from the blue dashed line. An arrow shows the position of the saturation intensity I_s, which is defined as the excitation intensity that makes the scattering cross-section becomes half of the small-signal value (shown by the black dotted line). (d) Saturation intensity with different excitation wavelengths, manifesting that saturation of scattering is dominated by SPR properties.

Back to Figure 1b, in the region between 2×10^5 and 4×10^5 W/cm^2, the scattering intensity has deviated from linear trend, but it still grows upward. However, in the range of 4×10^5 to 7×10^5 W/cm^2, the scattering intensity actually drops with increasing excitation intensity. The vertex occurs around 10^6 W/cm^2, where the scattering intensity in Figure 1b and the scattering cross-section in Figure 1c start to increase, presenting

dx.doi.org/10.1021/ph4000218 | ACS Photonics 2014, 1, 32−37

the onset of reverse saturable scattering (RSS). The slope quickly increases, and the scattering cross-section surpasses one around 2×10^6 W/cm^2.

The curve indicates interplay of mechanisms for SS and RSS and looks very similar to the result of SA and RSA in the literature[9,15] (see Figure 3b in ref 9 and Figure 4b in ref 15 by flipping their vertical axis as [1 − transmission]). It has been suggested that the physical origin of SA (or enhanced transmission) is "bleaching" of plasmon absorption due to hot electron generation by light,[15] resulting in modification of the dielectric function of the nanoparticle, and thus the corresponding scattering is also saturated.

On the other hand, the possible mechanisms of RSA (or reduced transmission) include photodegradation of the nanostructure,[16] the transient absorption from the free carriers,[15,17] and the enhanced light scattering process.[18] In the photodegradation mechanism, the transmission at a particular wavelength is reduced because the particle is degraded and SPR shifts. However, in this previous experiment, both nanorods and nanospheres were examined, and degradation is only observed with nanorods. Besides, we have confirmed that our SA and RSA are perfectly reversible and repeatable on a single nanosphere basis (see Figure 4), so we should exclude the photodegrade possibility. Another possibility is the transient two-photon absorption from free carriers. However, because there is no detectable two-photon luminescence in our result (see inset of Figure 1b), two-photon absorption is unlikely to be the dominating factor here. Note that in these earlier works, no measurement of scattering was performed. Our result provides direct evidence that scattering is significantly enhanced on a single-particle basis. According to our result in Figure 1c, in the RSS region, scattering cross-section becomes larger than the small signal value when excitation intensity is high. Since we detect backscattering, the stronger the scattering, the lower is the transmission. Therefore, our work offers a strong support to the explanation of reduced transmission based on enhanced light scattering at high intensity.

Similar to the analysis of SA and RSA,[7] we introduce nonlinearities into the scattering intensity equation, $I_{sca} = \alpha I + \beta I^2 + \gamma I^3 + \text{HOT}$, where I_{sca} and I are the scattering and excitation intensities, respectively; α is linear scattering coefficient; β and γ are nonlinear scattering coefficients, respectively; and HOT are higher-order terms that are not significant here. By fitting the data points, as shown by the green line in Figure 1b, we can quantitatively determine the relative values of β/α as 1.7×10^{-6} cm^2/W and γ/α as 9.4×10^{-11} cm^4/W^2, respectively. Compared to a saturable absorption report of gold nanoparticles with similar size,[19] the value of second order nonlinear absorption coefficient β_{abs} is in the range of 10^{-7}–10^{-10} cm/W. Since the typical value of linear absorption α_{abs} is on the order of 0.1 cm, the ratio of β_{abs}/α_{abs} is among 10^{-6}–10^{-9} cm^2/W. So our value of scattering based β/α fits into the value derived from absorption-based measurement, suggesting that SA and SS shares similar physical origin.

Different from an absorption measurement, which is typically carried out in forward collection scheme as an ensemble effect, scattering signals can be collected in the backward direction, and individual particles can be easily identified under a CLSM. Figure 2 shows the variation of PSF of backscattering signal at the focus of a CLSM with increasing excitation intensity at 561 nm. In Figure 2a, the left panel is an image showing several isolated gold nanoparticles with 80 nm diameter, and the right panel is an intensity profile corresponding to the white dashed line in the left panel. When laser intensity is less than 10^5 W/cm^2, no saturation of scattering is expected, so the PSF fits well to a Gaussian profile. In Figure 2b, the laser intensity at the peak is slightly higher than 10^5 W/cm^2, where saturation starts

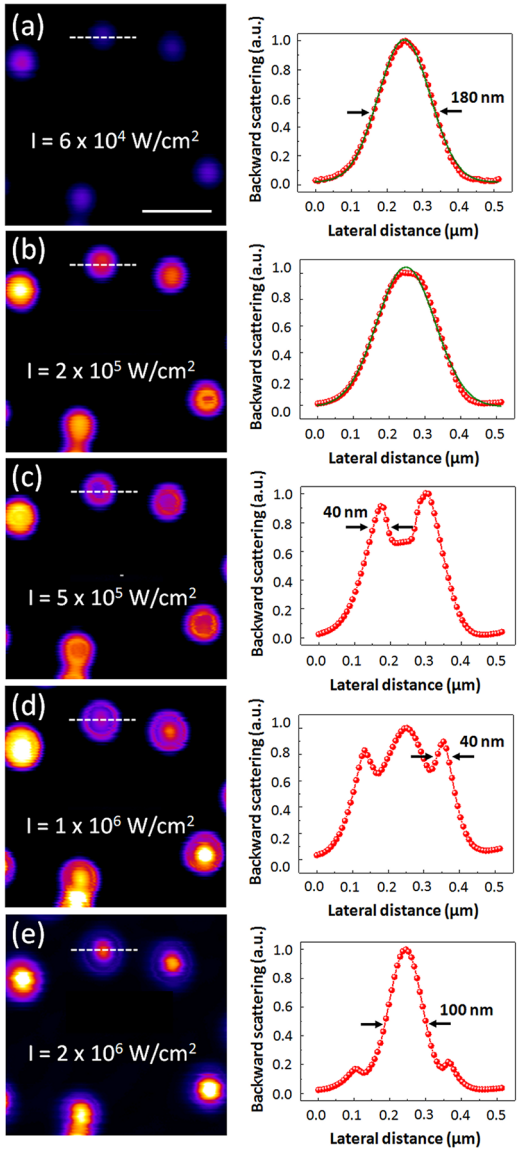

Figure 2. PSF of scattering from isolated gold nanoparticles evolves with increasing excitation intensity. The left column shows backscattering images and the right column gives the signal profile of a selected nanoparticle (white dashed line). The red circles are experimental values and green lines are Gaussian fitting. (a) When the excitation intensity is low, the PSF fits well to a Gaussian profile. (b) As the intensity is higher than 10^5 W/cm^2, the top of PSF becomes flattened, manifesting the onset of saturation. (c) With intensity keeps increasing, the saturation effect is stronger, resulting in the very interesting PSF that the center is lower than peripheral. The widths of the side lobes are about 40 nm. (d) When the intensity is higher than 10^6 W/cm^2, the scattering signal at the center of PSF increases again, revealing the onset of reverse saturation. (e) The reverse saturated scattering quickly dominates the PSF as the excitation continues to increase. The FWHM of the reverse saturated part is about 100 nm, showing great potential for high-resolution microscopy. Scale bar: 500 nm.

dx.doi.org/10.1021/ph4000218 | ACS Photonics 2014, 1, 32−37

to occur according to Figure 1b. Since only the intensity at the central part of PSF is high enough to induce saturation, the result of such a slight nonlinear effect is a flat top in the PSF, as we can see in the right panel of Figure 2b. Outside the center of focus, the peripheral part of the PSF still follows very well to a Gaussian profile.

When the peak intensity is increased to 5×10^5 W/cm^2, the scattering signal is in fact slightly reduced, producing a valley in the center of PSF. This result is in good agreement to Figure 1b. It is very interesting to notice that the side lobe of the valley exhibits a full-width-at-half-maximum (FWHM) around 40 nm, which is 4.5 times smaller than FWHM of the PSF in Figure 2a. In Figure 2d, where the peak intensity doubles and reaches the threshold for RSS, a clear increase of scattering signal is observed in the center of PSF. Note that the side lobe is still as narrow as in Figure 2c. In Figure 2e, the laser intensity reaches 2×10^6 W/cm^2, which is equivalent to less than 2 mW laser power at focus. Strong RSS is observed in the center of PSF. At this intensity, the RSS dominates the response, and the FWHM of the corresponding PSF is reduced to less than 100 nm, showing great potential in high-resolution microscopy.

The change of PSF in spatial domain can be deduced by a concept similar to transfer function, which links input and output. In this study, the connection between excitation intensity (input) and scattering intensity (output) is given in Figure 1b, which acts as a transfer function. The laser excitation intensity distribution in spatial domain is a Gaussian distribution, and thus with a given peak intensity, the excitation intensity at each spatial pixel is well-defined. The back-scattering PSF can then be obtained by substituting the excitation intensity distribution into the transfer function and calculating the corresponding output scattering signal at each pixel. A theoretical set of curves with different excitation intensities is shown in Figure 3, which nicely reproduces our observation in Figure 2.

Recently, there have been great successes in enhancing resolution of optical microscopy that can overcome a diffraction limit by exploiting the switching or saturation of fluorescence.[20−22] However, fluorescence suffers from photobleaching. On the other hand, scattering provides an attractive alternative contrast agent since it does not bleach. One possible direction is to combine SS and RSS with saturation-based super-resolution techniques, such as saturation excitation (SAX) microscopy[23] and saturated structured illumination microscopy (SSIM).[24]

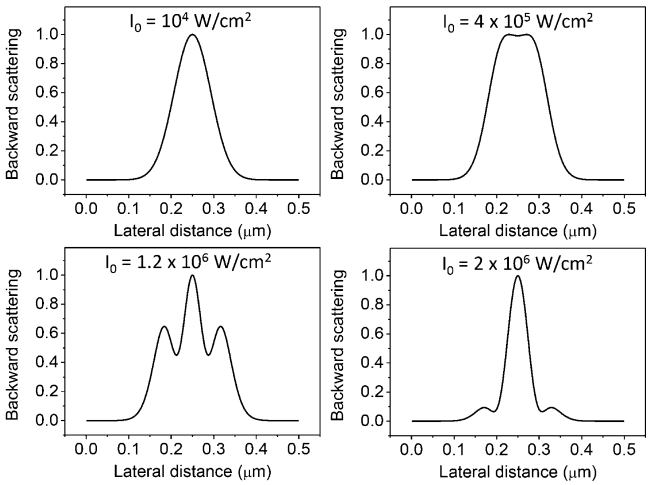

Figure 3. Using Figure 1b as a transfer function and using Gaussian intensity distribution with different peak intensities, the variation of PSF can be nicely reproduced.

To facilitate the imaging possibility, one major issue is the reversibility and repeatability of the saturation effect, because we used a relatively strong laser intensity to achieve saturation of scattering. In Figure 4, we demonstrate that the SS and RSS effects are not only reversible, but also repeatable on a single particle basis. To test the reversibility, we first increase the laser power to near 10^6 W/cm^2, so clear mountain-shaped point spread functions are seen in multiple particles in the first panel of Figure 4. Then the laser intensity gradually reduced to less than 10^5 W/cm^2, where the particle profiles come back to Gaussian, as shown in the middle row of Figure 4. This demonstrates that the saturation and reverse saturation of scattering is reversible. In the bottom row of Figure 4, the intensity is increased to 10^6 W/cm^2 again with the same set of particles. Clearly, we can see the PSFs evolve from flat-hat, to donut, to mountain shape, and finally to a narrow bright central lobe, manifesting that SS and RSS are repeatable on a single particle basis.

It is known that SA and RSA can be applied to all-optical signal processing. However, most previous SA and RSA experiments in plasmonic materials are performed with ensemble measurements. In this paper, we have suggested that the physical origin of SS and RSS is similar to that of SA and RSA, so SS and RSS should be applicable to all-optical signal processing with similar intensity levels of SA and RSA. The main advantage of SS and RSS over SA and RSA for signal processing is that the measurement of the former can be performed on a single particle basis. Single-particle SA has also been realized, but it requires a rather complicated setup.[12] With the reversibility and repeatability shown in Figure 4, we believe that SS and RSS of plasmonic particles will soon find applications in optical nanoscopy and all-optical signal processing on a nanometer scale.

As a final remark, it is interesting to notice that the value of saturation intensity in our experiment, which uses continuous-wave lasers, corresponds well to the value of SA with continuous-wave lasers.[12] But in the literature, the saturation intensity for SA induced by continuous-wave lasers seems to be much lower than that induced by femtosecond lasers.[9] It is known that the value of third-order susceptibility of gold nanoparticles measured with 70 ps pulses is around 30 times larger than the value measured with 200 fs pulses,[25] indicating that hot- electron nonlinearity requires at least a few picoseconds to rise. Therefore, it is not surprising that the saturation intensity of SA or SS is smaller with continuous-wave lasers. More detailed time-resolved experiments with femtosecond lasers will provide better insight for the mechanism of SS and RSS.

In summary, we have found that scattering from an isolated gold nanoparticle exhibits saturation and reverse saturation behaviors. A wavelength-dependent study reveals that the saturable scattering is governed by the SPR property of the nanoparticle. The nonlinear intensity dependency of scattering is analogous to the intensity dependence of absorption, manifesting that nonlinear scattering and nonlinear absorption share similar physical origins, including bleaching of ground-state plasmon absorption and subsequent enhanced scattering process. We demonstrated that the nonlinear behaviors of scattering dramatically change the PSF under a CLSM, and the

dx.doi.org/10.1021/ph4000218 | ACS Photonics 2014, 1, 32−37

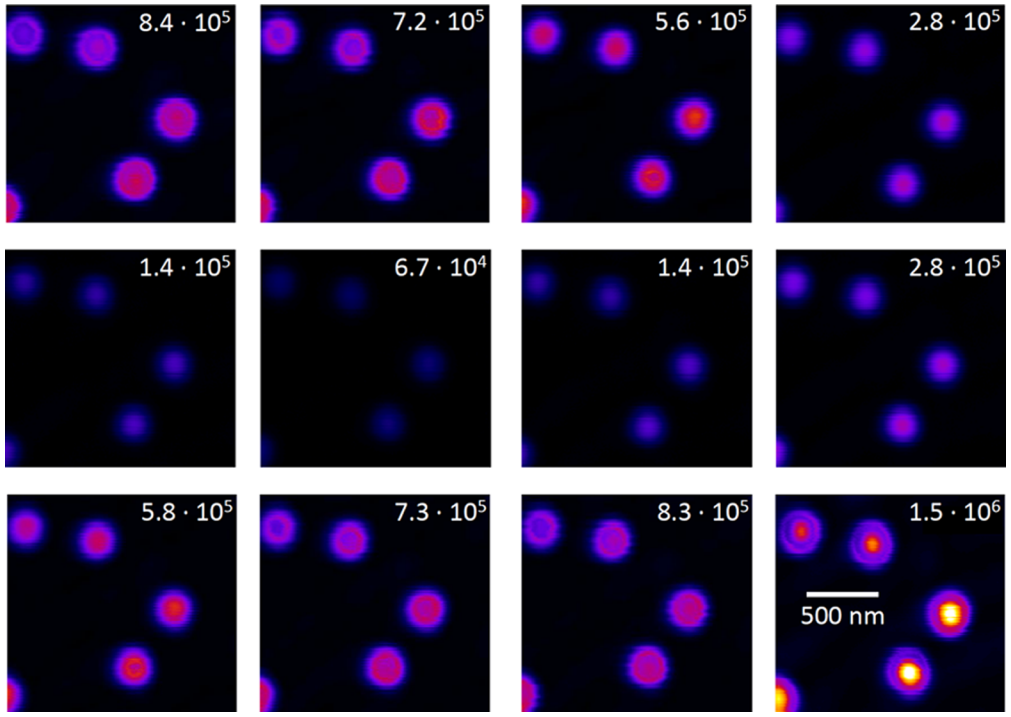

Figure 4. Reversible and repeatable SS and RSS effects. The numbers in each frame indicate the excitation intensity in W/cm^2.

nonlinear behaviors are reversible and reproducible. Our work presents a novel nonlinear phenomenon in fundamental light–matter interaction and will be potentially useful to nanophotonic applications as well as high-resolution microscopy.

AUTHOR INFORMATION

Corresponding Author

*E-mail: swchu@phys.ntu.edu.tw (S.-W.C.); fujita@ap.eng.osaka-u.ac.jp (K.F.).

Notes

The authors declare no competing financial interest.

ACKNOWLEDGMENTS

This study was supported by the National Science Council Grant NSC-101-2923-M-002-001-MY3. T.-Y.S. acknowledged the helpful financial support from the Ministry of Education, Taiwan. This research is also supported by the Japan Society for the Promotion of Science (JSPS) through the "Funding Program for Next Generation World-Leading Researchers (NEXT Program)," initiated by the Council for Science and Technology Policy (CSTP) and JSPS Asian CORE Program.

REFERENCES

(1) Lee, B.; Kim, S.; Kim, H.; Lim, Y. The use of plasmonics in light beaming and focusing. *Prog. Quant. Electron.* **2010**, *34* (2), 47–87.

(2) Lal, S.; Link, S.; Halas, N. J. Nano-optics from sensing to waveguiding. *Nature Photon.* **2007**, *1*, 641–648.

(3) Nezhad, M. P.; Simic, A.; Bondarenko, O.; Slutsky, B.; Mizrahi, A.; Feng, L. A.; Lomakin, V.; Fainman, Y. Room-temperature subwavelength metallo-dielectric lasers. *Nature Photon.* **2010**, *4* (6), 395–399.

(4) Fang, N.; Lee, H.; Sun, C.; Zhang, X. Sub-diffraction-limited optical imaging with a silver superlens. *Science* **2005**, *308* (5721), 534–537.

(5) Boyd, R. W. *Nonlinear Optics*, 2nd ed.; Elsevier: Singapore, 2003.

(6) Kauranen, M.; Zayats, A. V. Nonlinear plasmonics. *Nature Photon.* **2012**, *6* (11), 737–748.

(7) Ros, I.; Schiavuta, P.; Bello, V.; Mattei, G.; Bozio, R. Femtosecond nonlinear absorption of gold nanoshells at surface plasmon resonance. *Phys. Chem. Chem. Phys.* **2010**, *12* (41), 13692–13698.

(8) Link, S.; El-Sayed, M. A. Shape and size dependence of radiative, non-radiative and photothermal properties of gold nanocrystals. *Int. Rev. Phys. Chem.* **2000**, *19* (3), 409–453.

(9) Elim, H. I.; Yang, J.; Lee, J. Y.; Mi, J.; Ji, W. Observation of saturable and reverse- saturable absorption at longitudinal surface plasmon resonance in gold nanorods. *Appl. Phys. Lett.* **2006**, *88* (8), 083107.

(10) Wang, J.; Blau, W. J. Inorganic and hybrid nanostructures for optical limiting. *J. Opt. A: Pure Appl. Opt.* **2009**, *11* (2), 024001.

(11) Wada, O. Femtosecond all-optical devices for ultrafast communication and signal processing. *New J. Phys.* **2004**, *6*, 183.

(12) Chong, S. S.; Min, W.; Xie, X. S. Ground-state depletion microscopy: detection sensitivity of single-molecule optical absorption at room temperature. *J. Phys. Chem. Lett.* **2010**, *1* (23), 3316–3322.

(13) Bohren, C. F.; Huffman, D. R. *Absorption and Scattering of Light by Small Particles*; John Wiley & Sons, Inc.: Germany, 1983.

(14) Ahmadi, T. S.; Logunov, S. L.; El-Sayed, M. A. Picosecond dynamics of colloidal gold nanoparticles. *J. Phys. Chem.* **1996**, *100* (20), 8053–8056.

(15) Gurudas, U.; Brooks, E.; Bubb, D. M.; Heiroth, S.; Lippert, T.; Wokaun, A. Saturable and reverse saturable absorption in silver nanodots at 532 nm using picosecond laser pulses. *J. Appl. Phys.* **2008**, *104*, 073107.

(16) De Boni, L.; Wood, E. L.; Toro, C.; Hernandez, F. E. Optical saturable absorption in gold nanoparticles. *Plasmonics* **2008**, *3* (4), 171–176.

(17) Jiang, X. F.; Pan, Y. L.; Jiang, C. F.; Zhao, T. T.; Yuan, P. Y.; Venkatesan, T.; Xu, Q. H. Excitation nature of two-photon photoluminescence of gold nanorods and coupled gold nanoparticles studied by two-pulse emission modulation spectroscopy. *J. Phys. Chem. Lett.* **2013**, *4* (10), 1634–1638.

(18) West, R.; Wang, Y.; Goodson, T. Nonlinear absorption properties in novel gold nanostructured topologies. *J. Phys. Chem. B* **2003**, *107*, 3419–3426.

(19) Venkatram, N.; Kumar, R. S. S.; Rao, D. N.; Medda, S. K.; De, S.; De, G. Nonlinear optical absorption and switching properties of gold nanoparticle doped SiO_2-TiO_2 sol-gel films. *J. Nanosci. Nanotechnol.* **2006**, *6* (7), 1990−1994.
(20) Hell, S. W. Far-field optical nanoscopy. *Science* **2007**, *316* (5828), 1153−1158.
(21) Betzig, E.; Patterson, G. H.; Sougrat, R.; Lindwasser, O. W.; Olenych, S.; Bonifacino, J. S.; Davidson, M. W.; Lippincott-Schwartz, J.; Hess, H. F. Imaging intracellular fluorescent proteins at nanometer resolution. *Science* **2006**, *313* (5793), 1642−1645.
(22) Rust, M. J.; Bates, M.; Zhuang, X. W. Sub-diffraction-limit imaging by stochastic optical reconstruction microscopy (STORM). *Nat. Methods* **2006**, *3* (10), 793−795.
(23) Fujita, K.; Kobayashi, M.; Kawano, S.; Yamanaka, M.; Kawata, S. High-resolution confocal microscopy by saturated excitation of fluorescence. *Phys. Rev. Lett.* **2007**, *99* (22), 228105.
(24) Gustafsson, M. G. L. Nonlinear structured-illumination microscopy: Wide-field fluorescence imaging with theoretically unlimited resolution. *Proc. Natl. Acad. Sci. U.S.A.* **2005**, *102* (37), 13081−13086.
(25) Liao, H. B.; Xiao, R. F.; Fu, J. S.; Wang, H.; Wong, K. S.; Wong, G. K. L. Origin of third- order optical nonlinearity in Au: SiO_2 composite films on femtosecond and picosecond time scales. *Opt. Lett.* **1998**, *23* (5), 388−390.

dx.doi.org/10.1021/ph4000218 | *ACS Photonics* 2014, 1, 32−37